DR-WLC: Dimensionality Reduction cognition for object detection and pose estimation by Watching, Learning and Checking

Yu Gao^{1,2}, Xi Xu^{1,2}, Tianji Jiang^{1,2}, Siyuan Chen^{1,2}, Yi Yang*, Yufeng Yue^{1,2}, Mengyin Fu^{1,2}

Abstract—Object detection and pose estimation are difficult tasks in robotics and autonomous driving. Existing object detection and pose estimation methods mostly adopt the samedimensional data for training. For example, 2D object detection usually requires a large amount of 2D annotation data with high cost. Using high-dimensional information to supervise lower-dimensional tasks is a feasible way to reduce datasets size. In this work, the DR-WLC, a dimensionality reduction cognitive model, which can perform both object detection and pose estimation tasks at the same time is proposed. The model only requires 3D model of objects and unlabeled environment images (with or without objects) to finish the training. In addition, a bounding boxes generation strategy is also proposed to build the relationship between 3D model and 2D object detection task. Experiments show that our method can qualify the work without any manual annotations and it is easy to deploy for practical applications. Source code is at https: //github.com/IN2-ViAUn/DR-WLC.

I. INTRODUCTION

Object detection and pose estimation are widely used in unmanned driving, robot navigation and augmented reality. Existing 2D object detection and 3D pose estimation methods based on deep learning often require a large number of 2D image annotation datasets and 3D pose information for deep network training respectively. However, human usually do not have to traverse lots of object images and pose information in various scenes to complete the above tasks. We can reconstruct a 3D model only by simple observations in any scenes to guide us estimate poses and find boundary of objects. Inspired by this idea, we propose a dimensionality reduction cognitive model in this paper. The model can achieve object detection and pose estimation tasks in complex scenes only by 3D model of objects.

The architecture of our model can be divided into three stages: Watching, Learning and Checking.

In the Watching stage, we first use the designed 3D model observation strategy to generate ground-truth poses information, then EfficientNeRF(E-NeRF) is adopted to generate 2D images of objects by using the ground-truth poses. Finally, the morphological operation is used to obtain bounding boxes.

In the Learning stage, 2D images from different views are input into the improved Transformer-based object detector DETR-DR to get the prediction poses and bounding boxes.

The ground-truth poses and bounding boxes obtained in the Watching stage are used to supervise the training of network.

In the Checking stage, DETR-DR and E-NeRF are combined training to finetune the precision of poses. The unlabeled environment background images are introduced to further improve the robustness of practical environments. Fig. 1 visualizes this overall pipeline.

Frequent access to 3D model is basic requirement for our method. 3D reconstruction methods based on voxel [1], [2], mesh [3], point cloud [4], [5] often take a long time to build the model, and it is difficult to obtain dense and clear rendered images quickly from any views. Significantly, the NeRF [6]-series methods greatly improve the quality of rendered results. Although some works focus on improving NeRF towards more accurate [7] and larger reconstructed scenes [8], the high-resolution rendered results have less effect on object detection that pay more attention to object boundary. The recent works such as EfficientNeRF(E-NeRF) [9], FastNeRF [10] focus on the speed of model, which is a crucial factor to 3D model observation strategy design and implementation. In our method, it is acceptable to give up model rendering accuracy to some extent to greatly improve the rendering speed of images. In addition, since the NeRFseries methods store the model in an implicit way based on neural network, it can be embedded into existing networks, fixing network weights and participating in backpropagation and inference. In this paper, we adopt EfficientNeRF(E-NeRF) as the storage repository for 3D model.

The main contributions of our paper are the following:

- We propose a dimensionality reduction cognitive model, named DR-WLC, which can perform object detection and pose estimation using only 3D model of objects and unlabeled background images (with or without objects).
- A method of generating object ground truth boxes in simple scene is proposed, which build the relationship between 3D model and 2D object detection task.

The rest of the paper is organized as follows. Section II provides an overview of object detection methods, NeRF series methods and pose estimation methods. Section III introduces the principles of NeRF series methods and the implementation details of DR-WLC. The experiment results are shown in section IV. Finally, in section V we make a summary of our work.

II. RELATED WORK

A. Object Detection Methods

Object detection is an important research field of computer vision. CNN-based object detectors can be divided into

^{*}This work was partly supported by National Natural Science Foundation of China (Grant No. NSFC 61973034, 62233002, U1913203, 61903034 and CJSP Q2018229)

¹School of Automation, Beijing Institute of Technology, Beijing, China

²State Key Laboratory of Intelligent Control and Decision of Complex System, Beijing Institute of Technology, Beijing, China

^{*}Corresponding author: Y. Yang Email: yang yi@bit.edu.cn

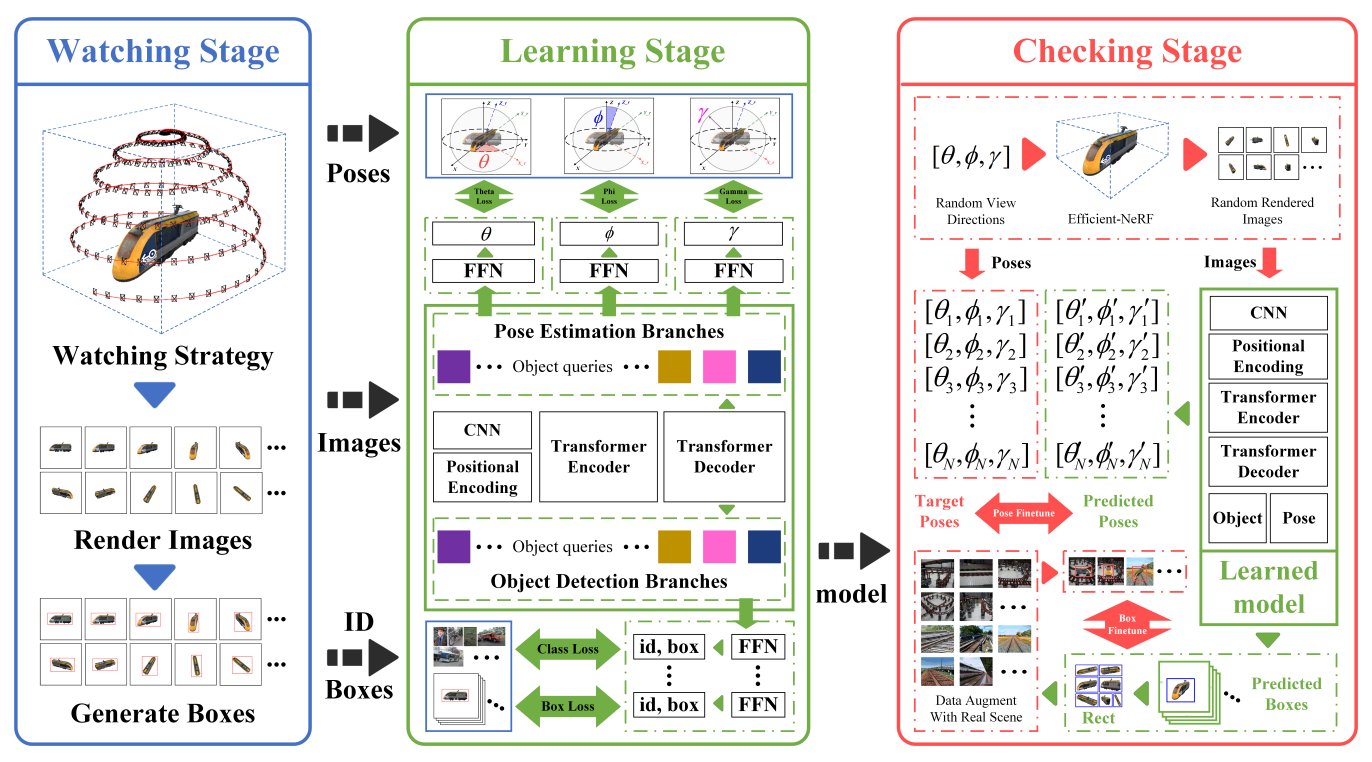


Fig. 1: The pipeline of proposed method. The architecture of our work consists of three parts. The Watching stage is to generate training data of simple scenes, including raw images with poses and bounding boxes. The Learning stage mainly conducts coarse training of the network to ensure the network has the primary ability to identify objects. In the Checking stage, the background images are used to synthesize complex scenes data. The pre-trained network adopts augment data to finetune weights, which aims to enhance the robustness for complex scenes. It is worth noting that we employ the pre-trained E-NeRF as 3D model repository acting as a supervisor. E-NeRF only participates in forward calculation without any network weight adjustment.

anchor-based detectors and anchor-free detectors. The R-CNN series methods [11]–[14], some of the YOLO series methods [15]–[18], SSD [19], RetinaNet [20] all use the anchor mechanism. The newly released YOLOv7 [18] surpasses many previous research works in speed and accuracy. However, anchor mechanism not only reduce the generalization ability but also increase the amount of extra computation. Besides, anchor mechanism also lead to problems, such as imbalance of positive and negative samples.

The anchor-free detectors can directly predict objects without pre-setting anchor boxes. Although the researchers pay more attention to anchor-based detectors than anchor-free detectors in the early stage, such as anchor-free mechanism adopted in DenseBox [21] and YOLOv1 [22] are not inherited in the following works, the design ideas laid the foundation for the future work. In general, anchor-free algorithms can be divided into dense prediction methods [23]–[26], and keypoint-based methods [27]–[29]. Both of them can achieve the comparable performance as the anchor-based algorithms while avoiding the defects of the anchor mechanism.

In recent years, with the successful application of Transformer from NLP to CV, some Transformer-based object detectors flourished. DETR [30] achieves the successful combination of CNN and Transformer. Deformable DETR

[31] borrowed the idea of deformable convolution and used a multi-scale deformable attention module. These design effectively improved the problems of DETR, such as training speed and poor detection effect on small objects.

B. NeRF Series Methods

Neural Radiation Field [6] adopts neural networks to implicitly describe 3D space. The impressive accuracy and elegant design of NeRF attract great attention. However, NeRF requires a large amount of data and expensive training cost. To improve the speed, it is feasible to change the MLP, which is the most time consuming part. For example, introducing a voxel grid with a small network for implicit storage and rendering [32], [33], or taking neural 3D point cloud [34], or even abandon the network structure directly [35]. Reducing the number of sampling points can also improve rendering speed [9], [36]. In addition, there are some works that use bake-like methods to achieve acceleration [37]-[41], which transfer the trained model to some structures that can render quickly. Impressive results have also been achieved with the aid of mathematical tools to improve network performance [10], [42]. Reducing the dependence on a large amount of data is also an important research direction for NeRF. There are two common ways, one is to improve the network structure or training method, such as Mip-NeRF [43], infoNeRF [44], etc. The other is to use the scene prior learned by the network, and then perform fine-tuning for the new input [45]–[48]. Application of NeRF is also an interesting research field. In terms of navigation, NeRF is used as a map, and position estimation is performed based on RGB or depth information [49]–[52]. At the same time, researchers are also exploring NeRF-related principles and techniques in other fields, such as scene editing [53], style transfer [54].

C. Pose Estimation Methods

6DoF pose estimation is a key technology for realizing vehicle automatic driving and robot object grasping. The purpose is to complete the transformation from the object coordinate system to the camera coordinate system. The traditional object pose estimation need to use PnP methods to solve the correspondence between 3D-2D point pairs. But since the PnP problem is not differentiable at some points [55], it becomes difficult to learn all points and weights in an end-to-end manner. Recently, EPro-PnP proposed by Chen et al. [56] makes the PnP problem derivable by introducing a probability density distribution, which greatly enhances the adaptability of the monocular object pose estimation model. The deep learning- based 6DoF pose estimation work no longer relies on 3D template matching [57]. Pose estimation methods based on convolutional neural networks [58], [59] and keypoint detection [60], [61] have developed rapidly and achieved ideal performance. In addition, pose estimation can also be performed through point cloud information, such as Frustum-PointNet [62] and Voxelnet [63].

III. METHOD

In this section, we first review the basic principles of NeRF and why we choose E-NeRF as the 3D model supervisor. Then, we introduce the details of our method.

A. Background

The basic idea of NeRF [6] is that given a set of images of a scene with known view directions, a neural network adopts these information for training, and implicitly model the scene. The new view images of the scene are generated by volume rendering. Specifically, NeRF samples 3D point x=(x,y,z) along ray r, and takes direction $d=(\theta,\phi)$ of the sampling point as input. After MLP network (which can be regarded as the mapping function f), color c and volume density σ corresponding to the sampling point are output. The formula is

$$(\sigma, c) = f(x, d) \tag{1}$$

Using the principle of classical volume rendering and the method of numerical approximation, the integral is calculated along each ray passing through the scene. By obtaining the corresponding pixel color on the image plane, a 2D image under the viewing direction is rendered. In addition, NeRF introduces positional encoding, which maps the position and direction information to a high-dimensional space, and then inputs them into the neural network. Positional encoding can

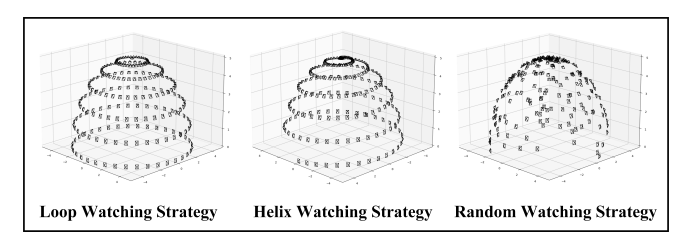


Fig. 2: The illustration of three watching strategies.

effectively solve the poor performance of NeRF in expressing high-resolution complex scenes. In terms of rendering strategy, NeRF adopts "coarse to fine" hierarchical voxel sampling, and samples finer points based on the probability density function generated during coarse stage. NeRF optimizes both coarse and fine networks by minimizing the mean square error of each corresponding pixel color(denoted by C(r) and $\widehat{C}(r)$ respectively) between ground truth image and rendered image, formulated as:

$$L = \sum_{r \in R} \|C(r) - \widehat{C}(r)\|_2^2$$
 (2)

where R is the set of all camera rays.

However, NeRF spends a lot of time during training and rendering, which is not conducive to the application. There are some researches currently devoted to improving NeRF in terms of speed [9], [32]–[41]. Among them, E-NeRF [9] improves the training speed through effective sampling and key sampling in coarse stage and fine stage respectively. The designed NerfTree, a 2-depth tree data structure, is employed to cache coarse dense voxels and fine sparse voxels extracted from coarse and fine MLP. This allows for faster inference by directly querying voxels for density and color. E-NeRF can greatly reduce the amount of computation and shorten training and inference time while maintaining accuracy.

B. Watching Stage

There are two main challenges of the Watching Stage:

- How to design the watching strategy to obtain the ground-truth pose and rendered images. Under the condition of using less data, the performance of DETR-DR is guaranteed.
- How to automatically generate label of bounding boxes to avoid manual labeling.

Fig. 2 shows three watching strategies: Loop Strategy, Helix Strategy, and Random Strategy. As defined in NeRF, θ and ϕ represent view direction, while γ represents the rendering radius of the E-NeRF model. All watching points are sampled from the 3D sphere formed by γ . The Loop Strategy divides ϕ equally into M parts, where each part corresponds to one watching loop. And θ is equally divided into N parts. The Helix Strategy divides θ and ϕ equally into N and M watching points respectively. These points are combined in a helix line way to generate a watching route. It should be noted that when evaluating these strategies, it is necessary to ensure these strategies have the same number of watching points. When the watching strategy is determined,

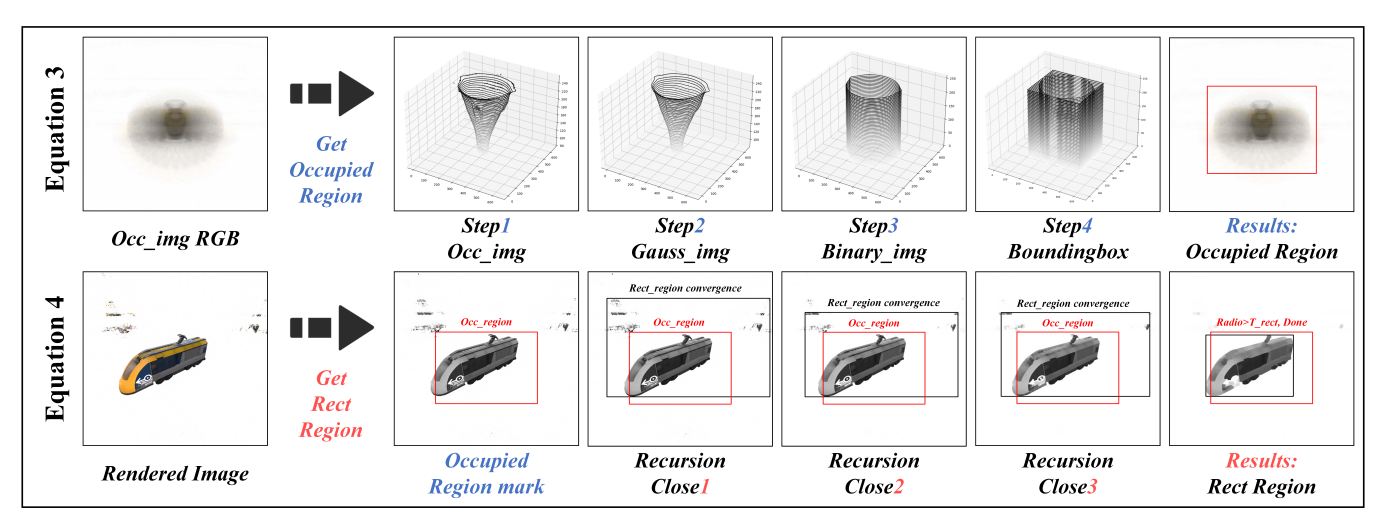


Fig. 3: **The generation process of the ground-truth boxes.** The first line illustrates how to obtain the *occupied region*. The second line shows the recursive method for *Rect region*.

pose information $(\theta, \phi \text{ and } \gamma)$ and corresponding rendered images generated by E-NeRF are regarded as ground truth labels and enter the Learning stage.

We adopt morphological algorithm to generate label of bounding boxes. Since the background of rendered images obtained by the Nerf series methods is relatively solid, as shown in Fig. 3 *Rendered Image*, the morphology can meet the requirements of data generation. We superimpose rendered images with weights to obtain occupied region of objects. The process is shown in Equation 3:

$$\begin{cases} Step1: Occ_img = \sum_{i=0}^{N} (img_RGB_i/N) \\ Step2: Gauss_img = Gauss(Gray(Occ_img)) \\ Step3: Binary_img = Binary(Gauss_img, T) \\ Step4: Occ_region = BBox(Binary_img) \end{cases}$$
(3)

Where N represent the images and the total number of images produced by the watching strategy respectively. Gray means converting RGB images to grayscale images. Gauss stands for Gaussian filtering. Binary and T represent binary operation and the threshold. BBox means to calculate the bounding rectangle. Occ_region is the occupied region. The first line of Fig. 3 illustrates the pipeline of algorithm.

The function of the occupied region is to decide whether the boxes generated by each image is available. Although we can obtain solid background with E-NeRF, there is still noise existing due to the E-NeRF performance, as shown in the second line of Fig. 3. The morphological close operation can filter out the interference area, but the noise generated by different images is relatively random, which is difficult to adopt a single threshold for all close operations. Therefore, we use recursive method to increase the size of close kernel gradually to meet the requirements of bounding boxes generation for different images. The process is shown in Equation 4. Where *Close* represents the morphological close operation. *kernel* is the size of close operation kernel. *T_Single* means the binarization threshold for each image. *inter* represents the intersection operation, which is the same as it in IoU. *Area* means the area calculation.

C. Learning Stage

In the Learning stage, we mainly introduce the DETR-DR model, data augmentation and loss functions.

DETR-DR is modified by the Transformer-based object detector DETR. As shown in the Learning stage of Fig. 1, the classic DETR network only contains object detection branches, which are used to predict classes and bounding boxes. We add the pose estimation branches only by modifying the outputs of DETR for predicting θ , ϕ , and γ . An important reason for employing DETR as the basic model is that the complete design stages we proposed have no strict restrictions to the network structure, but have strict restrictions to prediction box format. The object detectors such as YOLO-series methods need NMS to get the final bounding box results, which is difficult to find the corresponding relationship to poses during the training process.

$$\begin{cases} Step1: Gray_img = Gray(img_RGB) \\ Step2: Binary_img = Binary(Close(Gray_img, kernel), T_single) \\ Step3: temp_region = BBox(Binary_img) \\ Step4: radio = inter(temp_region, Occ_region)/Area(temp_region) \\ Step5: \begin{cases} rect_region = temp_region, radio > T_rect \\ Gray_img = Close(Gray_img), kernel + +, return Step2 \end{cases}$$

$$(4)$$

As for data augmentation, we randomly choose the operation of shift, scaling and random background color. In terms of the loss functions, classes prediction and bounding boxes regression adopt cross entropy loss and GIOU loss respectively, which are the same as DETR. And the pose regression is performed by L1 loss.

D. Checking Stage

The Checking stage focus on two tasks. One is to finetune the weights of pose estimation branches, the other is to enhance the robustness of the object detection branches to the environment.

The DETR-DR model trained by a small amount of ground-truth pose generated in the Watching stage have poor performance for practical applications. In the Checking stage, E-NeRF and DETR-DR models are jointly trained. Firstly, a large amount of random poses feed into E-NeRF to get rendered images. Secondly, the images are fed into DETR-DR to predict poses and bounding boxes. Finally, the pose estimation performance is finely optimized by the loss between the predicted pose and the random pose. In the pose finetune loss function, γ still uses L1 loss. θ and ϕ are regarded as the width and height of image respectively, and the IoU loss is calculated as shown in Equation 5.

$$\begin{cases}
Inter = \min(\theta_{prd}, \theta_{trt}) \cdot \min(\phi_{prd}, \phi_{trt}) \\
Loss = 1 - \frac{Inter}{\theta_{prd} \cdot \phi_{prd} + \theta_{trt} \cdot \phi_{trt} - Inter}
\end{cases} (5)$$

where θ_{prd} and ϕ_{prd} represent the predicted poses. θ_{trt} and ϕ_{trt} represent the ground-truth poses.

In order to enhance the robustness of complex scenes, a large number of scene images are introduced as background without any annotation. The bounding boxes surrounded regions predicted by DETR-DR are cut out to generate *Rect*. The *Rect* are randomly shifted, scaled, and fused with background images to generate a new dataset. Since the regions unoccupied by objects of *Rect* are solid, the fusion can be done with morphological and AND operation, which only has small impact on the scene images. It should be noted that the above composite images are only used for training the object detection branches and do not participate in pose finetune. The object detection branches fine-tuning loss function is GIOU.

IV. EXPERIMENTS AND RESULTS

In this section, we explain the details in the experiments and present the results.

A. Experimental Environment and Equipments

We adopt the locomotive in LEGO-60197 as the experimental model. The designed special data acquisition equipment is used to collect the training data of E-NeRF. The equipment consists of three observation loops. The interval angle ϕ of each observation loop is 30°, and there are 16 camera view points in each loop with an interval θ of 22.5°. The top layer of the equipment is a regular octagonal

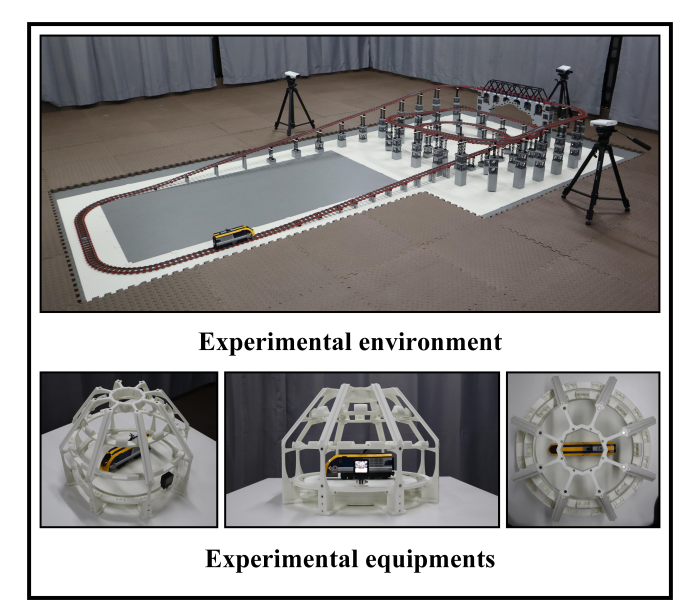


Fig. 4: Experimental environment and equipments.

structure with 4 camera view points at 90° intervals. We designed and built the LEGO rail viaduct as experimental environment. Data are acquired using the RGB mode of Kinect Azure cameras. Specifically as shown in Fig. 4.

B. Watching Strategy Experiment

We analyze the effects of three watching strategies. The evaluation results are shown in Table I. **View Points** represents the number of sampled viewpoints. **Step** means the resolution of angle. **mAP** (mean Average Precision) is used to evaluate object detection performance. **Ave deg** represents the average angle error to evaluate the results of pose regression. γ is fixed and equal to the observation radius of E-Nerf.

We use 1800 images randomly generated by E-Nerf as evaluation dataset. The method employed to generate bounding boxes is the same as it in the Watching stage. The specific parameters: $T_occ = 0.95 \cdot max(Gauss_img) = 242.25$, $T_single = 0.9 \cdot max(Gray_img) = 229.5$, $T_rect = 0.75$. The training epochs of all strategies are 1000 with the same learning rate of 0.001.

Four groups of comparative experiments with different parameters are adopted to evaluate the Watching strategy. With the increase of viewpoints number, the performance of three strategies are all improved, which means the number of viewpoints is a decisive factor. We use global average method to comprehensively evaluate these strategies under the condition of the same number of viewpoints. As shown in the blue font of Table I, the Random strategy has great advantage.

C. Detection and Pose Estimation Evaluation

In order to verify the fine-tuning effect of the Checking stage, we compare the performance of DETR-DR pass through different stages, as shown in Table II. **Strategy**

TABLE I: The evaluation results of three watching strategies.

Strategy	View Points	Step (deg°) $\theta \in [0, 360)$ $\phi \in [0, 90)$	mAP	Ave deg (deg°)			
				θ	ϕ	γ	
Loop	144	θ step: 10 ϕ step: 30	0.558	37.445	6.177	0.694	
Helix	144		0.577	35.100	6.911	0.705	
Random	144	,	0.509	23.961	3.460	0.541	
Loop	288	θ step: 5 ϕ step: 30	0.523	17.235	5.881	0.610	
Helix	288		0.576	20.037	5.459	0.652	
Random	288	φ στορ. σσ	0.584	15.961	2.296	0.568	
Loop	252	θ step: 10 ϕ step: 15	0.517	15.475	3.450	0.628	
Helix	252		0.432	19.286	2.203	0.652	
Random	252	φ στορί 15	0.586	21.657	2.465	0.542	
Loop	504	θ step: 5 ϕ step: 15	0.472	11.806	4.208	0.602	
Helix	504		0.650	6.981	3.163	0.615	
Random	504	<i>ү</i> жер. те	0.523	10.371	2.327	0.583	
Strategy	Global mAP	Global Ave-θ	Globa	l Ave-φ	Global	Ave- γ	
Loop	0.518	20.490	4.929		0.634		
Helix	0.559	20.351	4.434		0.656		
Random	0.551	17.988	2.637		0.559		

TABLE II: The evaluation results of different stages.

A.B. G.	Gr. 4	4 D	Ave deg (deg°)		
After Stage	Strategy	mAP	θ	ϕ	γ
Learning	Loop[θ:2°, φ: 5°]	0.772	9.676	3.222	0.582
	Helix[θ :2°, ϕ : 5°]	0.831	9.789	2.017	0.518
	Random][All: 3420]	0.804	7.018	1.896	0.613
Checking	Loop][θ:2°, φ: 5°]+R[5000]	0.798	5.959	1.864	0.615
	Helix][θ :2°, ϕ : 5°]+R[5000]	0.843	3.261	1.156	0.606
	Random][θ :2°, ϕ : 5°]+R[5000]	0.850	1.981	0.977	0.507

represents the combination of strategies adopted by DETR-DR. **R** means the number of random view points chose during the joint training process. γ is fixed and equal to the observation radius of E-Nerf.

We generate 5400 new images randomly by E-NeRf as evaluation dataset. The dataset is different from it used in Watching Strategy Experiment, but the parameters in data generation and training process are the same as those in Watching Strategy Experiment.

Compared with Table I, the trend of indicators in Table II is relatively clear. the performance of random strategy is still the best with the re-training process provided by Checking stage, both the performance of object detection and pose estimation are improved greatly. The results show that the Checking stage is effective and necessary.

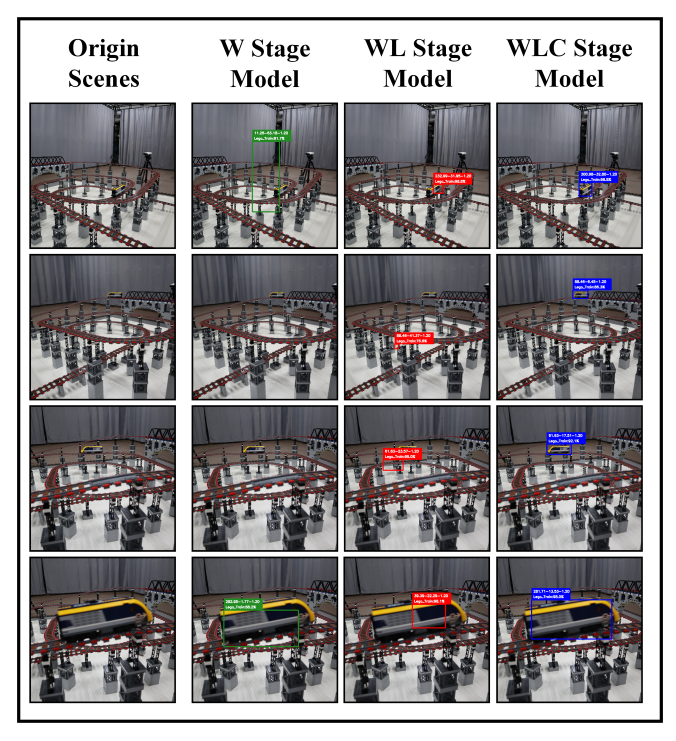


Fig. 5: Detection results in real scenes generated by DETR-DR trained on different stages. The first column shows original images. The second column shows the results provided by the model only trained with E-NeRF rendered images without data augmentation (the same training strategy with Table I experiment). The third and last columns show the results after the Learning and checking stage respectively.

D. Detection and Pose Estimation in real scene

Different from the object detection method trained on public datasets (COCO, KITTI, PASCAL VOC), our method is not able to obtain all 3D models of detected objects in the datasets. This makes it difficult to use the public datasets for evaluation. In addition, our training process have no humanlabeled annotations, which means there are no ground-truth poses and boxes of objects in the test scene. Therefore, we only present the prediction results as shown in Fig. 5.

V. CONCLUSION

In this work, we propose a dimensionality reduction cognitive model, named DR-WLC, which can perform object detection and pose estimation at the same time. The method only adopt 3D model of objects and unlabeled environment images (with or without objects) as the datasets for training, and make it suitable for practical applications. Inspired by the implicit network structure of NeRF-series models, we successfully embed EfficientNeRF as a supervisor into the complete training process to achieve joint training. In addition, we propose a method to generate ground-truth boxes for NeRF-series rendering images. The basic relationship between 3D model and 2D object detection task is built. The experiments demonstrate the effectiveness of DR-WLC, and also prove that our method is feasible in engineering.

ACKNOWLEDGMENT

The authors would like to thank Jiadong Tang, Zhaoxiang Liang, Hao Liang, Daiwei Li and all other members of ININ Lab of Beijing Institute of Technology for their contribution to this work.

REFERENCES

- [1] D. Eigen, C. Puhrsch, and R. Fergus, "Depth map prediction from a single image using a multi-scale deep network," *Advances in neural information processing systems*, vol. 27, 2014.
- [2] C. B. Choy, D. Xu, J. Gwak, K. Chen, and S. Savarese, "3d-r2n2: A unified approach for single and multi-view 3d object reconstruction," in *European conference on computer vision*, pp. 628–644, Springer, 2016.
- [3] N. Wang, Y. Zhang, Z. Li, Y. Fu, W. Liu, and Y.-G. Jiang, "Pixel2mesh: Generating 3d mesh models from single rgb images," in *Proceedings* of the European conference on computer vision (ECCV), pp. 52–67, 2018.
- [4] H. Fan, H. Su, and L. J. Guibas, "A point set generation network for 3d object reconstruction from a single image," in *Proceedings of the IEEE conference on computer vision and pattern recognition*, pp. 605–613, 2017.
- [5] R. Chen, S. Han, J. Xu, and H. Su, "Point-based multi-view stereo network," in *Proceedings of the IEEE/CVF international conference* on computer vision, pp. 1538–1547, 2019.
- [6] B. Mildenhall, P. P. Srinivasan, M. Tancik, J. T. Barron, R. Ramamoorthi, and R. Ng, "Nerf: Representing scenes as neural radiance fields for view synthesis," *Communications of the ACM*, vol. 65, no. 1, pp. 99– 106, 2021.
- [7] H. Luo, A. Chen, Q. Zhang, B. Pang, M. Wu, L. Xu, and J. Yu, "Convolutional neural opacity radiance fields," in 2021 IEEE International Conference on Computational Photography (ICCP), pp. 1–12, IEEE, 2021.
- [8] M. Tancik, V. Casser, X. Yan, S. Pradhan, B. Mildenhall, P. P. Srinivasan, J. T. Barron, and H. Kretzschmar, "Block-nerf: Scalable large scene neural view synthesis," in *Proceedings of the IEEE/CVF Conference on Computer Vision and Pattern Recognition*, pp. 8248–8258, 2022.
- [9] T. Hu, S. Liu, Y. Chen, T. Shen, and J. Jia, "Efficientnerf efficient neural radiance fields," in *Proceedings of the IEEE/CVF Conference* on Computer Vision and Pattern Recognition, pp. 12902–12911, 2022.
- [10] S. J. Garbin, M. Kowalski, M. Johnson, J. Shotton, and J. Valentin, "Fastnerf: High-fidelity neural rendering at 200fps," in *Proceedings* of the IEEE/CVF International Conference on Computer Vision, pp. 14346–14355, 2021.
- [11] R. Girshick, J. Donahue, T. Darrell, and J. Malik, "Rich feature hierarchies for accurate object detection and semantic segmentation," in *Proceedings of the IEEE conference on computer vision and pattern* recognition, pp. 580–587, 2014.
- [12] R. Girshick, "Fast r-cnn," in Proceedings of the IEEE international conference on computer vision, pp. 1440–1448, 2015.
- [13] S. Ren, K. He, R. Girshick, and J. Sun, "Faster r-cnn: Towards realtime object detection with region proposal networks," Advances in neural information processing systems, vol. 28, 2015.
- [14] K. He, G. Gkioxari, P. Dollár, and R. Girshick, "Mask r-cnn," in Proceedings of the IEEE international conference on computer vision, pp. 2961–2969, 2017.
- [15] J. Redmon and A. Farhadi, "Yolo9000: better, faster, stronger," in Proceedings of the IEEE conference on computer vision and pattern recognition, pp. 7263–7271, 2017.
- [16] J. Redmon and A. Farhadi, "Yolov3: An incremental improvement," arXiv preprint arXiv:1804.02767, 2018.
- [17] A. Bochkovskiy, C.-Y. Wang, and H.-Y. M. Liao, "Yolov4: Optimal speed and accuracy of object detection," arXiv preprint arXiv:2004.10934, 2020.
- [18] C.-Y. Wang, A. Bochkovskiy, and H.-Y. M. Liao, "Yolov7: Trainable bag-of-freebies sets new state-of-the-art for real-time object detectors," arXiv preprint arXiv:2207.02696, 2022.
- [19] W. Liu, D. Anguelov, D. Erhan, C. Szegedy, S. Reed, C.-Y. Fu, and A. C. Berg, "Ssd: Single shot multibox detector," in *European conference on computer vision*, pp. 21–37, Springer, 2016.

- [20] T.-Y. Lin, P. Goyal, R. Girshick, K. He, and P. Dollár, "Focal loss for dense object detection," in *Proceedings of the IEEE international* conference on computer vision, pp. 2980–2988, 2017.
- [21] L. Huang, Y. Yang, Y. Deng, and Y. Yu, "Densebox: Unifying landmark localization with end to end object detection," arXiv preprint arXiv:1509.04874, 2015.
- [22] J. Redmon, S. Divvala, R. Girshick, and A. Farhadi, "You only look once: Unified, real-time object detection," in *Proceedings of the IEEE* conference on computer vision and pattern recognition, pp. 779–788, 2016
- [23] C. Zhu, Y. He, and M. Savvides, "Feature selective anchor-free module for single-shot object detection," in *Proceedings of the IEEE/CVF* conference on computer vision and pattern recognition, pp. 840–849, 2019.
- [24] Z. Tian, C. Shen, H. Chen, and T. He, "Fcos: Fully convolutional one-stage object detection," in *Proceedings of the IEEE/CVF international conference on computer vision*, pp. 9627–9636, 2019.
- [25] T. Kong, F. Sun, H. Liu, Y. Jiang, L. Li, and J. Shi, "Foveabox: Beyound anchor-based object detection," *IEEE Transactions on Image Processing*, vol. 29, pp. 7389–7398, 2020.
- [26] Z. Ge, S. Liu, F. Wang, Z. Li, and J. Sun, "Yolox: Exceeding yolo series in 2021," arXiv preprint arXiv:2107.08430, 2021.
- [27] H. Law and J. Deng, "Cornernet: Detecting objects as paired keypoints," in *Proceedings of the European conference on computer vision* (ECCV), pp. 734–750, 2018.
- [28] X. Zhou, D. Wang, and P. Krähenbühl, "Objects as points," arXiv preprint arXiv:1904.07850, 2019.
- [29] X. Zhou, J. Zhuo, and P. Krahenbuhl, "Bottom-up object detection by grouping extreme and center points," in *Proceedings of the IEEE/CVF* conference on computer vision and pattern recognition, pp. 850–859, 2019
- [30] N. Carion, F. Massa, G. Synnaeve, N. Usunier, A. Kirillov, and S. Zagoruyko, "End-to-end object detection with transformers," in European conference on computer vision, pp. 213–229, Springer, 2020.
- [31] X. Zhu, W. Su, L. Lu, B. Li, X. Wang, and J. Dai, "Deformable detr: Deformable transformers for end-to-end object detection," arXiv preprint arXiv:2010.04159, 2020.
- [32] C. Sun, M. Sun, and H.-T. Chen, "Direct voxel grid optimization: Super-fast convergence for radiance fields reconstruction," in *Proceedings of the IEEE/CVF Conference on Computer Vision and Pattern Recognition*, pp. 5459–5469, 2022.
- [33] L. Wu, J. Y. Lee, A. Bhattad, Y.-X. Wang, and D. Forsyth, "Diver: Real-time and accurate neural radiance fields with deterministic integration for volume rendering," in *Proceedings of the IEEE/CVF* Conference on Computer Vision and Pattern Recognition, pp. 16200– 16209, 2022.
- [34] Q. Xu, Z. Xu, J. Philip, S. Bi, Z. Shu, K. Sunkavalli, and U. Neumann, "Point-nerf: Point-based neural radiance fields," in *Proceedings of the IEEE/CVF Conference on Computer Vision and Pattern Recognition*, pp. 5438–5448, 2022.
- [35] S. Fridovich-Keil, A. Yu, M. Tancik, Q. Chen, B. Recht, and A. Kanazawa, "Plenoxels: Radiance fields without neural networks," in *Proceedings of the IEEE/CVF Conference on Computer Vision and Pattern Recognition*, pp. 5501–5510, 2022.
- [36] F. Cole, K. Genova, A. Sud, D. Vlasic, and Z. Zhang, "Differentiable surface rendering via non-differentiable sampling," in *Proceedings* of the IEEE/CVF International Conference on Computer Vision, pp. 6088–6097, 2021.
- [37] L. Wang, J. Zhang, X. Liu, F. Zhao, Y. Zhang, Y. Zhang, M. Wu, J. Yu, and L. Xu, "Fourier plenoctrees for dynamic radiance field rendering in real-time," in *Proceedings of the IEEE/CVF Conference on Computer Vision and Pattern Recognition*, pp. 13524–13534, 2022.
- [38] C. Reiser, S. Peng, Y. Liao, and A. Geiger, "Kilonerf: Speeding up neural radiance fields with thousands of tiny mlps," in *Proceedings of the IEEE/CVF International Conference on Computer Vision*, pp. 14335–14345, 2021.
- [39] A. Yu, R. Li, M. Tancik, H. Li, R. Ng, and A. Kanazawa, "Plenoctrees for real-time rendering of neural radiance fields," in *Proceedings of the IEEE/CVF International Conference on Computer Vision*, pp. 5752– 5761, 2021.
- [40] P. Hedman, P. P. Srinivasan, B. Mildenhall, J. T. Barron, and P. Debevec, "Baking neural radiance fields for real-time view synthesis," in *Proceedings of the IEEE/CVF International Conference on Computer Vision*, pp. 5875–5884, 2021.

- [41] H. Wang, J. Ren, Z. Huang, K. Olszewski, M. Chai, Y. Fu, and S. Tulyakov, "R2l: Distilling neural radiance field to neural light field for efficient novel view synthesis," arXiv preprint arXiv:2203.17261, 2022
- [42] T. Müller, A. Evans, C. Schied, and A. Keller, "Instant neural graphics primitives with a multiresolution hash encoding," arXiv preprint arXiv:2201.05989, 2022.
- [43] J. T. Barron, B. Mildenhall, M. Tancik, P. Hedman, R. Martin-Brualla, and P. P. Srinivasan, "Mip-nerf: A multiscale representation for anti-aliasing neural radiance fields," in *Proceedings of the IEEE/CVF International Conference on Computer Vision*, pp. 5855–5864, 2021.
- [44] M. Kim, S. Seo, and B. Han, "Infonerf: Ray entropy minimization for few-shot neural volume rendering," in *Proceedings of the IEEE/CVF* Conference on Computer Vision and Pattern Recognition, pp. 12912– 12921, 2022.
- [45] N. Müller, A. Simonelli, L. Porzi, S. R. Bulò, M. Nießner, and P. Kontschieder, "Autorf: Learning 3d object radiance fields from single view observations," in *Proceedings of the IEEE/CVF Conference* on Computer Vision and Pattern Recognition, pp. 3971–3980, 2022.
- [46] D. Rebain, M. Matthews, K. M. Yi, D. Lagun, and A. Tagliasacchi, "Lolnerf: Learn from one look," in *Proceedings of the IEEE/CVF Conference on Computer Vision and Pattern Recognition*, pp. 1558–1567, 2022.
- [47] A. Yu, V. Ye, M. Tancik, and A. Kanazawa, "pixelnerf: Neural radiance fields from one or few images," in *Proceedings of the IEEE/CVF* Conference on Computer Vision and Pattern Recognition, pp. 4578– 4587, 2021.
- [48] S. Cai, A. Obukhov, D. Dai, and L. Van Gool, "Pix2nerf: Unsupervised conditional p-gan for single image to neural radiance fields translation," in *Proceedings of the IEEE/CVF Conference on Computer Vision* and Pattern Recognition, pp. 3981–3990, 2022.
- [49] Z. Zhu, S. Peng, V. Larsson, W. Xu, H. Bao, Z. Cui, M. R. Oswald, and M. Pollefeys, "Nice-slam: Neural implicit scalable encoding for slam," in *Proceedings of the IEEE/CVF Conference on Computer Vision and Pattern Recognition*, pp. 12786–12796, 2022.
- [50] L. Yen-Chen, P. Florence, J. T. Barron, A. Rodriguez, P. Isola, and T.-Y. Lin, "inerf: Inverting neural radiance fields for pose estimation," in 2021 IEEE/RSJ International Conference on Intelligent Robots and Systems (IROS), pp. 1323–1330, IEEE, 2021.
- [51] M. Adamkiewicz, T. Chen, A. Caccavale, R. Gardner, P. Culbertson, J. Bohg, and M. Schwager, "Vision-only robot navigation in a neural radiance world," *IEEE Robotics and Automation Letters*, vol. 7, no. 2, pp. 4606–4613, 2022.
- [52] E. Sucar, S. Liu, J. Ortiz, and A. J. Davison, "imap: Implicit mapping and positioning in real-time," in *Proceedings of the IEEE/CVF International Conference on Computer Vision*, pp. 6229–6238, 2021.
- [53] A. Kundu, K. Genova, X. Yin, A. Fathi, C. Pantofaru, L. J. Guibas, A. Tagliasacchi, F. Dellaert, and T. Funkhouser, "Panoptic neural fields: A semantic object-aware neural scene representation," in Proceedings of the IEEE/CVF Conference on Computer Vision and Pattern Recognition, pp. 12871–12881, 2022.
- [54] T. Nguyen-Phuoc, F. Liu, and L. Xiao, "Snerf: stylized neural implicit representations for 3d scenes," arXiv preprint arXiv:2207.02363, 2022.
- [55] F. Manhardt, D. M. Arroyo, C. Rupprecht, B. Busam, T. Birdal, N. Navab, and F. Tombari, "Explaining the ambiguity of object detection and 6d pose from visual data," in *Proceedings of the IEEE/CVF International Conference on Computer Vision*, pp. 6841–6850, 2019.
- [56] H. Chen, P. Wang, F. Wang, W. Tian, L. Xiong, and H. Li, "Epropnp: Generalized end-to-end probabilistic perspective-n-points for monocular object pose estimation," in *Proceedings of the IEEE/CVF Conference on Computer Vision and Pattern Recognition*, pp. 2781–2790, 2022.
- [57] S. Hinterstoisser, V. Lepetit, S. Ilic, S. Holzer, G. Bradski, K. Konolige, and N. Navab, "Model based training, detection and pose estimation of texture-less 3d objects in heavily cluttered scenes," in *Asian conference* on computer vision, pp. 548–562, Springer, 2012.
- [58] A. Kendall, M. Grimes, and R. Cipolla, "Posenet: A convolutional network for real-time 6-dof camera relocalization," in *Proceedings of* the IEEE international conference on computer vision, pp. 2938–2946, 2015
- [59] Y. Xiang, T. Schmidt, V. Narayanan, and D. Fox, "Posecnn: A convolutional neural network for 6d object pose estimation in cluttered scenes," arXiv preprint arXiv:1711.00199, 2017.
- [60] Y. He, W. Sun, H. Huang, J. Liu, H. Fan, and J. Sun, "Pvn3d: A deep point-wise 3d keypoints voting network for 6dof pose estimation,"

- in Proceedings of the IEEE/CVF conference on computer vision and pattern recognition, pp. 11632–11641, 2020.
- [61] S. Peng, Y. Liu, Q. Huang, X. Zhou, and H. Bao, "Pvnet: Pixel-wise voting network for 6dof pose estimation," in *Proceedings of the IEEE/CVF Conference on Computer Vision and Pattern Recognition*, pp. 4561–4570, 2019.
- [62] C. R. Qi, W. Liu, C. Wu, H. Su, and L. J. Guibas, "Frustum pointnets for 3d object detection from rgb-d data," in *Proceedings of the IEEE* conference on computer vision and pattern recognition, pp. 918–927, 2018
- [63] Y. Zhou and O. Tuzel, "Voxelnet: End-to-end learning for point cloud based 3d object detection," in *Proceedings of the IEEE conference on* computer vision and pattern recognition, pp. 4490–4499, 2018.